Exchange bias in disordered granular systems

2007 J. Phys.: Condens. Matter 19 225007

(http://iopscience.iop.org/0953-8984/19/22/225007)

IOP PUBLISHING JOURNAL OF PHYSICS: CONDENSED MATTER

J. Phys.: Condens. Matter **19** (2007) 225007 (17pp) doi:10.1088/0953-8984/19/22/225007

Exchange bias in disordered granular systems

D Fiorani[1], L Del Bianco[2], A M Testa[1] and K N Trohidou[3]

[1] Istituto di Struttura della Materia-CNR, 00016 Monterotondo Scalo, Roma, Italy
[2] Dipartimento di Fisica, Università di Bologna and CNISM, I-40127 Bologna, Italy
[3] Institute of Materials Science, NCSR Demokritos, 15310 Athens, Greece

E-mail: dino.fiorani@ism.cnr.it

Received 2 October 2006, in final form 4 December 2006
Published 14 May 2007
Online at stacks.iop.org/JPhysCM/19/225007

Abstract

The exchange bias properties of a granular system composed of Fe nanoparticles (mean size ∼6 nm) embedded in a structurally and magnetically disordered oxide have been investigated. The exchange bias field, resulting from the exchange coupling between the ferromagnetic particles and the frozen spin-glass-like oxide, strongly depends on the magneto-thermal history and ageing of the sample. Such dependence is a consequence of the magnetically disordered nature of the oxide phase and it is explained by considering that different frozen spin configurations of the oxide are selected on varying the temperature and the field-cooling process and that they evolve with the application time of the cooling field. Monte Carlo simulations on core/shell nanoparticles (ferromagnetic core/disordered ferrimagnetic shell) well reproduce the ageing effect.

1. Introduction

Since its discovery on Co/CoO nanoparticles in 1956 [1], the exchange bias (EB) effect has been the object of continuous interest from a fundamental point of view and for its potential in technological applications (magnetic sensors, spin-valve-based reading heads). However, despite the enormous efforts in theory, modelling and experimental investigations, especially on ferromagnet(FM)/antiferromagnet(AFM) bilayer systems, many questions on the microscopic mechanism of the phenomenon are still open [2]. The effect occurs when the FM/AFM system is cooled through the Néel temperature (T_N) of the AFM, the Curie temperature of the FM (T_C) being higher than T_N. Below T_N, the spins of the AFM couple to those of the FM so as to minimize the interface exchange interaction. Through the FM–AFM exchange interaction, a single stable configuration for the FM spins is induced and then a unidirectional anisotropy appears (exchange anisotropy). When the sample is cooled through T_N in a static magnetic field (H_{cool}), the exchange anisotropy manifests itself in the form of a shift of the hysteresis loop

usually towards negative H values (exchange bias). The value of the shift is conventionally taken as an estimate of the exchange field H_{ex}.

So far, the research in this field has been mainly focused on layered systems, allowing control of the FM and AFM thickness and of the interface structural features (crystallographic orientation, stoichiometry, roughness) [2]. New challenging questions were posed by the observation of EB on nanoparticle systems, where one phase is ferromagnetic (FM) and the other one is a spin glass (SG) [2, 3], playing the role of the antiferromagnet (AF) in pinning the FM magnetization so as to minimize the interface exchange interaction energy. Key examples of these systems are $NiFe_2O_4$ [3] and NiO [4] nanoparticles, which are composed of an ordered core (ferrimagnetic (FI), or antiferromagnetic, respectively) and a structurally and magnetically disordered surface shell, showing spin-glass-like properties. For these systems, the exchange bias phenomenon is expected to exhibit peculiar and unique features, directly related to the intrinsic energy structure and to the characteristic spin dynamics of the SG phase [5]. As the frozen SG state is characterized by the existence of multiple equivalent spin configurations, separated by a distribution of energy barriers, the exchange bias phenomenon in ordered/SG systems is expected to exhibit different characteristics with respect to FM/AFM systems, where only two energetically equivalent spin configurations exist for the AFM component.

When the FM/SG system is cooled down in a magnetic field (H_{cool}) across the glass temperature, a spin configuration of the SG phase will be selected, among the possible ones, through the interface exchange coupling with the FM phase, which in turn favours the FM magnetization to be aligned in the field-cooling direction (unidirectional anisotropy). Depending on the value of the cooling field and on the temperature at which it is applied, the degeneracy of the SG state can be reduced (actually, strong enough magnetic fields can destroy the SG state entirely). Thus the cooling field and the whole magneto-thermal history of the sample are expected to strongly affect the EB properties [6].

A further characteristic of the SG state, as well as of other disordered systems characterized by a collective non-equilibrium spin dynamics, is the ageing effect, i.e. the slowing down of the spin dynamics with increasing the time (waiting time) spent in the frozen state, before any field variation [7, 8]. Below the glass temperature, the relaxation rate of the zero-field-cooled magnetization (M_{ZFC}) and of the thermoremanent magnetization (TRM) decreases with increasing the time elapsing before the application of the magnetic field and the time of application of the cooling magnetic field before removing it, respectively. The effect reflects the shift, towards longer times, of the spectrum of relaxation times (which is associated to the distribution of energy barriers), due to the evolution of the system towards a lower-energy configuration. Thus, in FM/SG systems, ageing effects too are expected to affect the EB properties.

In this context, we have investigated the dependence of the exchange bias properties on magneto-thermal history and dynamical effects in a nanogranular disordered system composed of iron nanoparticles dispersed in a structurally and magnetically disordered iron oxide.

2. Results and discussion

2.1. Material preparation and structural properties

Fe nanoparticles were produced by the inert gas condensation (IGC) method [9]: 99.98% purity Fe was evaporated in a tungsten boat located in a chamber filled with He at a pressure of 133 Pa. Aerosol iron nanoparticles accumulated on a metallic rotating drum cooled by liquid N_2; then they were exposed to a mixture of 133 Pa O_2 and 1200 Pa He for 12 h to achieve passivation [10].

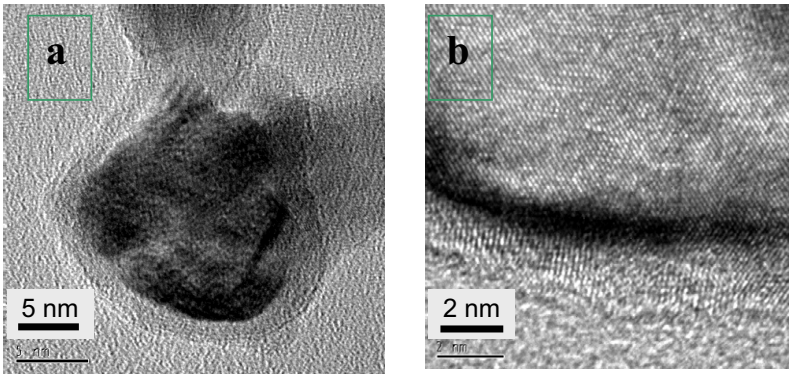

Figure 1. (a) TEM micrograph of an oxygen-passivated Fe nanoparticle. (b) Detail showing the oxide layer around the metallic core.

Figure 1 shows the transmission electron microscopy (TEM) micrograph of a typical Fe particle obtained by IGC and oxygen passivation (in this case, the nanoparticles were collected on a carbon-coated copper grid put inside the evaporation chamber during the synthesis process). The dark core corresponds to metallic iron whereas the surrounding light grey layer is the oxide phase. The thickness of such layer is ∼2 nm, independently of the Fe core size. The TEM contrast of the oxide phase resembles that of an amorphous structure and the presence of crystallites in this small region is hardly detectable (figure 1, right panel). The interface region between the metallic core and the oxide phase appears as a rather sharp boundary due to Fresnel fringes. The as-prepared particles are not always distinguishable as singular and well-separated entities, as shown in figure 1(a). More generally, the products of the evaporation and passivation procedures are agglomerates of several nanoparticles.

Nanoparticles with increasing mean size have been obtained by increasing the current crossing the tungsten boat, and hence the vapour temperature, during three evaporation processes. After the passivation, the particles were scraped from the cold finger and pressed in high vacuum with a uniaxial pressure of 1.5 GPa, to obtain the pellets labelled D6, D10 and D15, which were analysed by x-ray diffraction (XRD). The results are shown in figure 2. Two components are detected: the peaks of bcc Fe and the broadened and overlapping peaks of the oxide phase. The position and the integrated intensity of the latter correspond to the values usually given for magnetite (Fe_3O_4) and maghemite (γ-Fe_2O_3), both having spinel structure. However, the peak broadening does not allow us to distinguish between them.

The XRD patterns have been analysed following the Rietveld method [11] to determine the volume-averaged grain size D of the iron phase (providing a measure of the mean size of the Fe cores) and its weight fraction (a spinel structure for the oxide phase was assumed). In samples D6, D10 and D15, $D = 5.6$ nm (Fe weight fraction $x_{Fe} = 18 \pm 3\%$), $D = 9.6$ nm ($x_{Fe} = 28 \pm 3\%$) and $D = 15.2$ nm ($x_{Fe} = 59 \pm 3\%$) respectively (the error on D is 10%).

For the oxide lattice parameter, the Rietveld analysis provides an intermediate value between those of magnetite and maghemite (8.399–8.335 Å). Indeed, we cannot exclude that the oxide phase is a mixture of both Fe_3O_4 and γ-Fe_2O_3, as suggested in various research works on similar samples [12, 13]. The mean grain size of the oxide phase is ∼2 nm and the microstrain is of the order of 10^{-2}, consistent with a high structural disorder. The compacted sample can indeed be modelled as a collection of Fe particles embedded in a poorly crystallized oxide: actually, as a core–shell nanoparticle composite, in which the oxide shells are in contact.

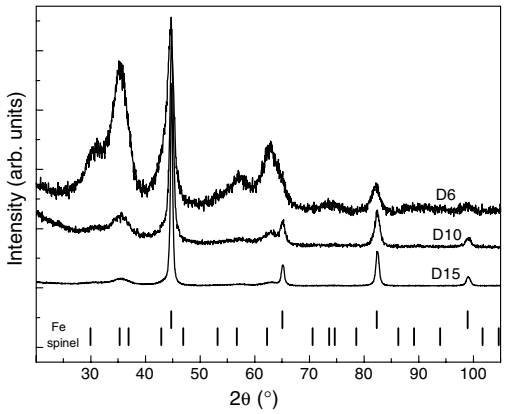

Figure 2. XRD spectra for samples D6, D10 and D15.

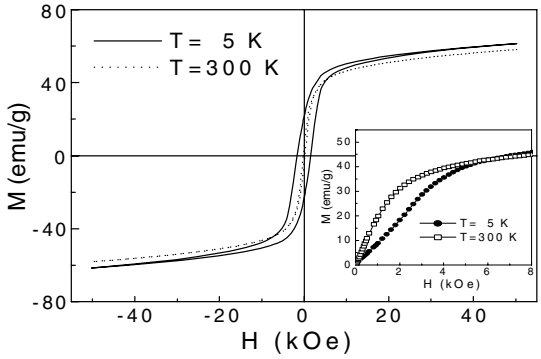

Figure 3. Magnetization loops at $T = 5$, 300 K. Inset: initial magnetization curves as a function of magnetic field at $T = 5$, 300 K.

2.2. Susceptibility and hysteresis cycles measurements

The magnetization (M) measurements were carried out with a commercial SQUID magnetometer (maximum applied field $H_{\text{appl}} = 50$ kOe) in the temperature range 5–300 K. If not differently specified, the following data refer to the D6 sample.

Hysteresis loops at $T = 5, 300$ K are shown in figure 3 (in the inset, the initial magnetization curves are displayed). The loops do not saturate. They show a rapid increase of magnetization at low fields, followed by a linear variation in the high-field region. This suggests the coexistence of an easily saturating component and a non-saturating highly anisotropic component, responsible for the high irreversibility field H_{irr} ($H_{\text{irr}} \sim 28$ kOe) at 5 K (H_{irr} is the magnetic field value above which the two branches of the loop in the first quadrant merge together in a single curve). The magnetization value at $H = 50$ kOe (61.4 emu g^{-1}) is well below the calculated one (110 emu g^{-1}), considering the Fe and oxide contents estimated by XRD. Such behaviour is consistent with a non-collinear spin arrangement and recalls that found in ferrimagnetic particles (γ-Fe_2O_3 [14, 15], $NiFe_2O_4$ [3]) where the coexistence of topological disorder and frustration of magnetic interactions at the surface resulted in spin-canting and spin-glass-like behaviour.

In our system too, magnetic disorder and frustration of magnetic interactions are present, due to the structurally disordered oxide matrix.

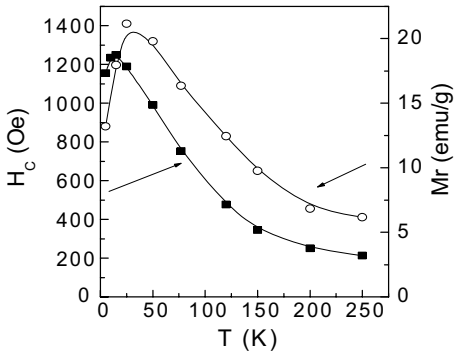

Figure 4. Coercivity H_c (closed symbols) and remanent magnetization M_r (open symbols) as a function of temperature.

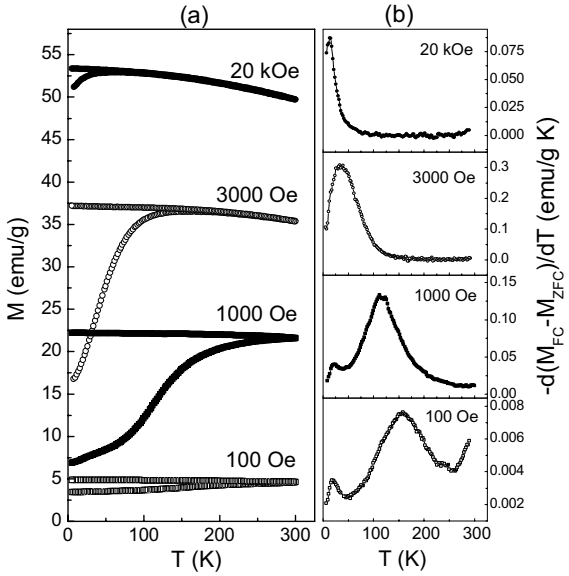

Figure 5. (a) Zero-field-cooled (ZFC, lower branch of each curve) and field-cooled (FC, upper branch) magnetization versus T for different $H_{\rm appl}$. (b) Temperature derivative $[-d(M_{\rm FC} - M_{\rm ZFC})/{\rm d}T]$ of the difference between FC and ZFC magnetization.

The coercivity H_c strongly increases with reducing T starting from $T \sim 150$ K (figure 4), reaching a maximum at ∼15 K. The remanent magnetization, M_r, shows the same behaviour, with a maximum at ∼25 K.

The zero-field-cooled ($M_{\rm ZFC}$) magnetization, and field-cooled ($M_{\rm FC}$) magnetization were measured versus T at different applied magnetic field (100 Oe $\leqslant H_{\rm appl} \leqslant$ 20 kOe; $M_{\rm ZFC}$ was measured on warming and $M_{\rm FC}$ during the subsequent cooling). Some results are shown in figure 5(a).

For $H_{\rm appl} < 1000$ Oe, magnetic irreversibility persists up to 250 K. We define $T_{\rm irr}$ as the temperature where the difference between $M_{\rm FC}$ and $M_{\rm ZFC}$, normalized to its maximum value at $T = 5$ K, becomes smaller than 3%. With increasing $H_{\rm appl}$, $T_{\rm irr}$ reduces and the shape of the $M_{\rm ZFC}$ changes, suggesting blocking/freezing phenomena at field-dependent

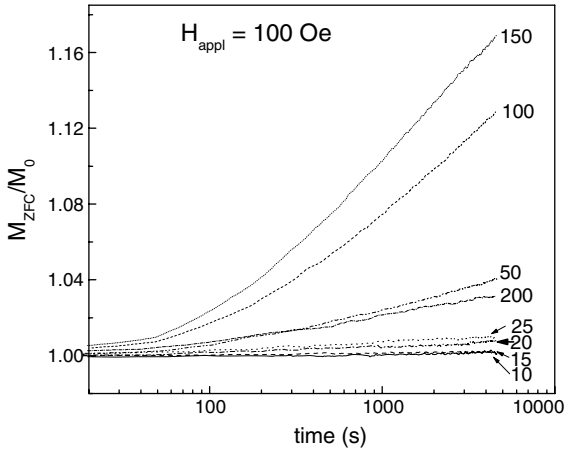

Figure 6. M_{ZFC} versus time for $H_{\mathrm{appl}} = 100$ Oe at the different temperatures. M_0 is the magnetization at the beginning of the measurements.

temperatures. In figure 5(b), the temperature derivative curves $[-d(M_{\mathrm{FC}} - M_{\mathrm{ZFC}})/\mathrm{d}T]$ are shown. It is worth recalling that, in the presence of independent relaxation phenomena (i.e. non-interacting particles), the temperature derivative of the remanent magnetization actually reflects the effective distribution of anisotropy energy barriers of the system [16]. Such a derivative curve has the same behaviour as the temperature derivative of the difference between M_{FC} and M_{ZFC}. Although in the present case the relaxation processes cannot be considered independent, qualitative information can be drawn from such analysis. A common feature of these curves is the presence of a weakly field-dependent peak at $T_1 \sim 20$ K, consistent with the presence of a frozen magnetic state for the whole system at low temperature. This is also confirmed by the lack of magnetic relaxation below $T = 25$ K, as shown in figure 6, where the time dependence of M_{ZFC} is reported at different temperatures ($H_{\mathrm{appl}} = 100$ Oe; note that the maximum of the relaxation rate relaxation is at $T = 150$ K).

A second large peak is observed at a temperature T_2 ($T_2 \sim 150$ K for $H_{\mathrm{appl}} = 100$ Oe): it becomes narrower and shifts to lower temperature with increasing field. In a simplified picture, we can describe our system as constituted by two components, strongly coupled at the interface: a non-relaxing (quasi-static) component (the Fe particles); and a relaxing magnetically disordered component (given by regions of exchange-interacting spins of the oxide matrix). Below T_1, the oxide region moments do not relax and are frozen in the spin-glass-like (or *cluster-glass-like*) state. On increasing the temperature above T_1, such moments become progressively unfrozen, according to the distribution of effective anisotropy energy barriers, determined by their size and the strength of the magnetic interaction with the surroundings. The large peak in the $[-d(M_{\mathrm{FC}} - M_{\mathrm{ZFC}})/\mathrm{d}T]$ curve at $H_{\mathrm{appl}} = 100$ Oe (figure 5(b)) reflects the width of such a distribution. It is worth noticing that magnetic irreversibility persists at low temperature even at $H_{\mathrm{appl}} = 20$ kOe. The results indicate that the hypothesized spin-glass-like state does not evolve in a pure paramagnetic or superparamagnetic regime with increasing T up to 300 K. Indeed, once the net moments of the oxide magnetic regions become able to thermally fluctuate, they tend to be polarized by the Fe particle moments, which thus prevent (or shift to higher temperature) the passage into the superparamagnetic regime. In fact, at $T = 300$ K the virgin M versus H curve is ferromagnetic-like. The polarizing action exerted by the Fe particle moments is boosted by the magnetic field, favouring the formation of a ferromagnetic

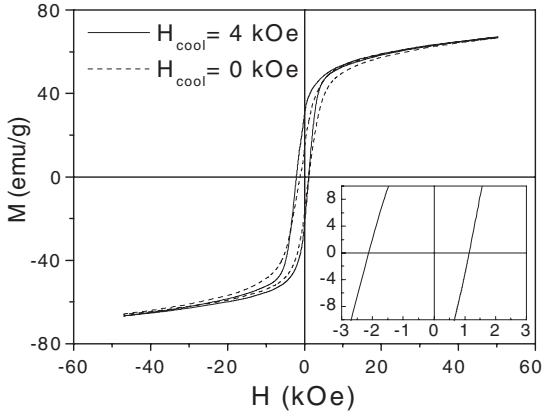

Figure 7. Hysteresis loops at $T = 5$ K after field cooling from $T_{\text{appl}} = 250$ K in $H_{\text{cool}} = 0$ (dotted line), 4 kOe (solid line). Inset: enlarged view of the central region of the loop at $H_{\text{cool}} = 4$ kOe.

network throughout the sample. On the other hand, at $T = 5$ K the curve is S-shaped, as found for frustrated systems [17] (figure 3, inset). The thermal evolution of H_c (figure 4) is coherent with the above picture: at very low temperature the frozen oxide matrix exerts a strong pinning action on the Fe particle moments, whereas at $T = 250$ K the oxide matrix is polarized by the Fe particles and its contribution to H_c can be neglected compared to that of the Fe particles.

Actually, at $T = 250$ K, the value of H_c is in agreement with that estimated by the Stoner–Wohlfarth model for randomly oriented, spherical single-domain Fe particles, $H_c = 0.64 \cdot K_{\text{Fe}}/M_S \sim 180$ Oe (K_{Fe}: magnetocrystalline anisotropy of bcc Fe; M_S: Fe saturation magnetization) [18]. Such a high value of H_c compared to that of compacted ferromagnetic nanoparticles [19] rules out the possibility that the Fe particle moments are ferromagnetically aligned by exchange interaction through the oxide. Actually, the oxide does not transmit the exchange interaction to neighbouring Fe particles.

2.3. Exchange bias properties

2.3.1. Temperature dependence. Field-cooled (FC) hysteresis loops were measured at different temperatures in the range 5–250 K on samples D6, D10 and D15 for different H_{cool} and compared with the corresponding cycles measured after zero-field cooling. In the field cooling procedure, the sample was cooled down from $T = 250$ K in a magnetic field. Once the measuring temperature was reached, the field was set at $H = 50$ kOe and the measurement of a hysteresis loop started. The hysteresis loops measured at 5 K after field cooling in $H = 4$ kOe and after zero-field cooling are reported in figure 7. A shift of the loop towards the negative field has been observed for the three samples. The shift is usually quantified through the positive exchange field parameter $H_{\text{ex}} = -(H_{\text{right}} + H_{\text{left}})/2$, H_{right} and H_{left} being the points where the loop intersects the field axis.

Figure 8 shows H_{ex} as a function of temperature for the D6, D10 and D15. H_{ex} increases with decreasing D, revealing that exchange anisotropy effects at the interface between particles and matrix are more important when the surface to volume ratio of the particles increases.

It is worth noting that for D6 H_{ex} appears below $T = 150$ K, i.e. in correspondence with the freezing of most of the moments of the oxide magnetic regions, as indicated by the value of T_2 in the $[-d(M_{\text{FC}} - M_{\text{ZFC}})/\text{d}T]$ curve at $H_{\text{appl}} = 100$ Oe (figure 5(b)); with reducing

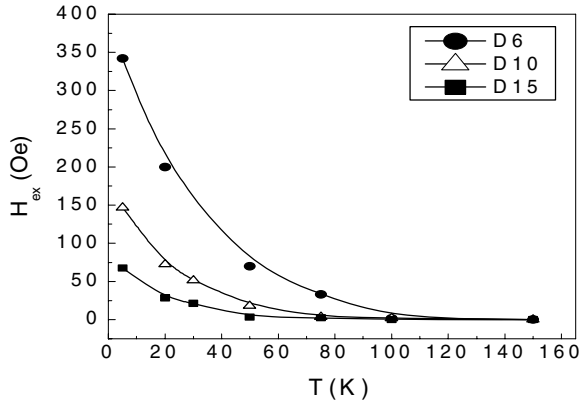

Figure 8. Exchange field (H_{ex}) as a function of temperature for samples D6, D10 and D15.

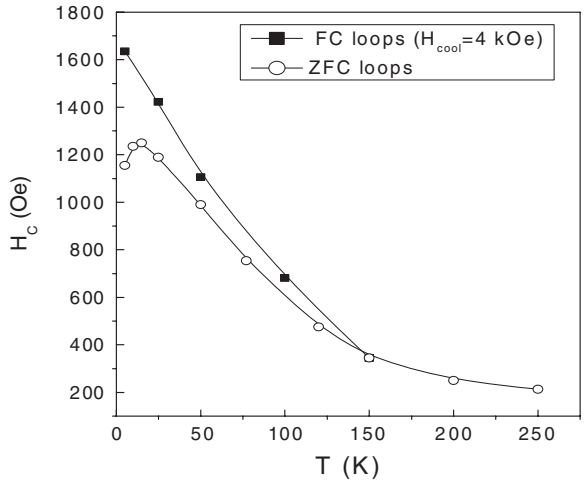

Figure 9. Coercive field versus temperature after zero-field cooling (open symbol) and field cooling at $H = 4$ kOe (solid symbol).

temperature below $T = 150$ K, H_{ex} shows a marked increase because of the progressive freezing of an increasing number of oxide region moments. Moreover, it can be noted that EB is accompanied by an increase of H_c, as shown in figure 9, where the H_c curve measured after field cooling splits from the ZFC one below 150 K.

To have an insight into the exchange bias phenomenon, a useful starting point is the Meiklejohn and Bean model, which predicts for FM/AFM systems the relation [20]

$$H_{ex} \cong J_{int}/M_{FM} \cdot t_{FM} \tag{1}$$

where J_{int} is the exchange constant across the FM/AFM interface per unit area and M_{FM} and t_{FM} are the magnetization and the thickness of the FM layer, respectively. It should be noted that important parameters are not considered in equation (1), such as the AFM layer anisotropy and thickness, the non-collinearity of the AFM–FM spins, and the formation of domains in the AFM and FM layers [2]. For real granular systems, the particle random orientation, the distribution of particle sizes and shapes, the difficulty to characterize the microstructure of the interface and, in our case, the spin-glass-like nature of the oxide, make it difficult to

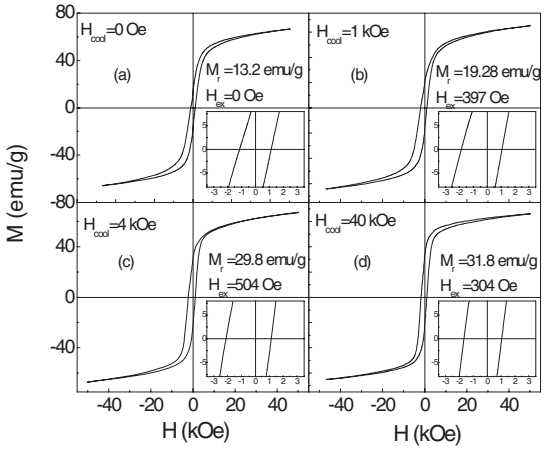

Figure 10. (a) Zero-field-cooled hysteresis loop measured at $T = 5$ K; (b)–(d) field-cooled hysteresis loops at $T = 5$ K for different cooling field ($H_{\rm cool}$). The remanent magnetization $M_{\rm r}$ and the coercivity $H_{\rm c}$ are reported. Insets: enlarged views of the central region of the loops.

extract quantitative information. Nevertheless, the observed increase of $H_{\rm ex}$ with decreasing D at $T = 5$ K (figure 8) constitutes an interesting result, resembling the $1/t_{\rm FM}$ dependence of equation (1). Moreover, a necessary condition for the observation of exchange anisotropy is [20]

$$K_{\rm AFM} \cdot t_{\rm AFM} \geqslant J_{\rm int} \tag{2}$$

where $K_{\rm AFM}$ and $t_{\rm AFM}$ are the anisotropy and the thickness of the AFM layer, respectively.

In our case, considering that the SG phase plays the role of the AF one, if one assumes for $M_{\rm FM}$ the value of bulk Fe (1714 emu cm^{-3}), for $t_{\rm FM}$ the mean particle size D and for $t_{\rm AFM}$ double the oxide shell thickness (∼4 nm, independently of D), equation (1) yields $J_{\rm int} = 0.35$ ergs cm^{-2} for sample D6 and then $K_{\rm AFM} \geqslant 9 \times 10^5$ ergs cm^{-3} from equation (2); for D15, $K_{\rm AFM} \geqslant 4 \times 10^5$ ergs cm^{-3}. Hence, the deduced $K_{\rm AFM}$, namely the oxide matrix anisotropy, is at least one order of magnitude larger than the magnetocrystalline anisotropy of bulk γ-Fe_2O_3 (4.6×10^4 ergs cm^{-3}) and definitely much larger than that of Fe_3O_4 (1×10^5 ergs cm^{-3}). Such estimation is close to the value found in γ-Fe_2O_3 nanoparticles (7×10^5 ergs cm^{-3}) and is associated with surface and finite size effects [21, 22].

2.3.2. Cooling field dependence. Hysteresis loops were measured at $T = 5$ K, for different values of $0 \leqslant H_{\rm cool} \leqslant 50$ kOe (figure 10). $M_{\rm r}$, $H_{\rm ex}$ and $H_{\rm c}$ (figure 11) strongly increase with $H_{\rm cool}$ up to $H_{\rm cool} = 4$ kOe: $M_{\rm r}$ and $H_{\rm c}$ increase by 127% and 46% respectively, with respect to the ZFC loop, and $H_{\rm ex} = 504$ Oe. Above $H_{\rm cool} = 4$ kOe, $M_{\rm r}$ reaches a plateau value of ∼30 emu g^{-1} whereas $H_{\rm ex}$ decreases monotonically down to ∼250 Oe for $H_{\rm cool} = 50$ kOe. $H_{\rm c}$ decreases at first and then it stabilizes around 1370 Oe, for $H_{\rm cool} \geqslant 20$ kOe.

The results can be explained within the following picture. At $T = 250$ K, $H_{\rm cool}$ aligns the Fe particle moments to a certain degree (depending on its value) and, with reducing T, the oxide moments freeze progressively, seeking the lowest energy configuration. Finally, at $T = 5$ K the whole system is frozen in a disordered state, determined by the complex interplay of matrix–particle (super)-exchange coupling and particle–particle dipolar interactions, which both can be ferromagnetic or antiferromagnetic in sign. Then, the field is increased from $H_{\rm cool}$ to $H = 50$ kOe and the loop measurement starts. Note that the direction of the applied field does not change and, at $H = 50$ kOe, $M \sim 66$ emu g^{-1}, independent of $H_{\rm cool}$ (figure 10).

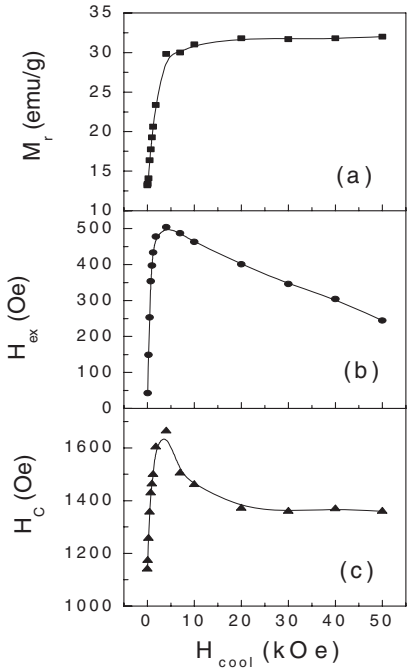

Figure 11. Remanent magnetization M_r (a), exchange field H_{ex} (b) and coercivity H_c (c), measured at $T = 5$ K, shown as a function of the cooling field (H_{cool}).

From figure 11, two different field regions can be distinguished:

• $H_{cool} < 4$ kOe

M_r increases (figure 11(a)), indicating that, although the sample's magnetization reaches during each loop measurement the same maximum value, the sample retains a magnetization that is higher for higher H_{cool}. The increase in M_r is accompanied by the increase in H_{ex} (figure 11(b)).

The exchange anisotropy at the interface between the single-domain metallic particles and the oxide sets in when the temperature is lowered across ∼140 K. In the demagnetized sample, as the Fe particle moments point in random directions, the exchange anisotropy is averaged out, and hence in the ZFC loop measurement at $T = 5$ K no shift is observed. Following the field-cooling process, due to the enhancement in the alignment degree of the Fe moments, the different contributions to the exchange anisotropy sum together and a net exchange bias effect can be observed.

The increase in H_c (figure 11(c)) with H_{cool} up to 4 kOe is coherent with the increase in H_{ex}: the field cooling induces a preferential direction along which the magnetic moments tend to freeze at $T = 5$ K, and thus the effect of averaging of the anisotropy, due to randomness, is reduced.

• $H_{cool} > 4$ kOe

M_r remains constant, whereas H_{ex} decreases monotonically. It should be considered that, with increasing H_{cool}, the magnetic coupling (Zeeman coupling) between the field and the oxide matrix moments increases as well, tending to orient them along the field direction. At $T = 5$ K, for high enough fields, such coupling may compete with the mix of magnetic interactions within the system, overcoming the exchange coupling at the interface between Fe particles and oxide matrix.

A similar explanation has been proposed to account for the positive exchange bias observed in FeF_2(AFM)–Fe(FM) bilayers [23]. It was found that for large cooling fields ($\geqslant$20 kOe) the loops of FeF_2(AFM)–Fe(FM) bilayers are shifted to positive fields, whereas, for small cooling fields, the usual shift towards the negative field was observed. The effect was explained by considering that the FeF_2–Fe interaction was antiferromagnetic and moreover that, for sufficiently high field, the coupling of the FeF_2 interface to the external cooling field overcomes the interface interaction between the two layers. The authors also assumed that the configuration of the antiferromagnetic layer remained fixed when the magnetic field was reversed. Hence the system was field-cooled into a high interface magnetic energy configuration and a positive exchange field resulted.

Similarly, in our case, it may be assumed that when the Zeeman coupling dominates on the magnetic interactions inside the system, for high enough fields, the system freezes in a configuration in which the energy associated with such internal interactions is not minimized. The oxide particle interface energy becomes higher and higher with increasing Zeeman coupling, which continuously increases with $H_{\rm cool}$, since the sample is not magnetically saturated even in $H = 50$ kOe (figure 7). Hence, $H_{\rm ex}$ decreases with increasing $H_{\rm cool}$, as is indeed observed (figure 11(b)).

Below $H_{\rm cool} = 4$ kOe, the Zeeman coupling should not be strong enough to compete with the matrix–particle exchange interaction and, in any case, its effect appears negligible compared to the increase in $H_{\rm ex}$ produced by the enhanced alignment of the particles moments, as results from the increase in $M_{\rm r}$.

Actually, $H^* = 4$ kOe can be considered an effective *depinning* threshold field above which magnetic interactions are overcome by the Zeeman coupling.

Above this field, due to the Zeeman coupling, the oxide matrix and the particles are less strongly exchange coupled, and thus the oxide exerts a weaker pinning on the particle moments, resulting in a decrease of the coercivity of the system (figure 11(c)). Unlike $H_{\rm ex}$, $H_{\rm c}$ cannot decrease indefinitely with $H_{\rm cool}$ since its value is determined by the anisotropy energy barriers that the frozen magnetic moments have to overcome in order to annihilate $M_{\rm r}$. The height of such anisotropy energy barriers, although affected by the strength of the magnetic interactions, is mainly determined by the intrinsic magnetic anisotropy of the system and by its microstructure. Hence, $H_{\rm c}$ approaches a constant value ($\sim$1370 Oe) for $H_{\rm cool} \geqslant 20$ kOe (figure 11(c)), where $M_{\rm r}$ is constant too (figure 11(a)).

2.3.3. The ageing effect dependence. The dynamical effects on the EB properties were investigated through the control of the ageing of the system (variation of the waiting time and cooling rate). Moreover, in order to gain a better insight into the origin of such dynamical effects, we have performed Monte Carlo (MC) simulations on isolated, spherical core(FM)/shell(FI) nanoparticles, as such simulations have shown the capability to predict waiting time effects and to reproduce complicated magnetization reversal modes [5, 24, 25]. The effect of the waiting time ($t_{\rm w}$) was analysed through the following experiment. The sample was cooled down in zero field from $T = 250$ K to $T_i = 50$ K. Then, $H_{\rm cool} = 4$ kOe was applied for a time $t_{\rm w}$ (in the 60–60 000 s range), before starting the field cooling down to $T_{\rm f} = 5$ K (cooling rate $= 5$ K min^{-1}). At $T_{\rm f}$, the hysteresis loop was measured, starting from $H = 50$ kOe. After each measurement, the sample was warmed up again to $T = 250$ K. The evolution of $M_{\rm r}$, $H_{\rm ex}$ and $H_{\rm c}$ with $t_{\rm w}$ is shown in figure 12 (right panel).

$H_{\rm ex}$ increases monotonically over 20% with increasing $t_{\rm w}$ (figure 12(b)). A small increase in M_r (figure 12(a)) is also observed. On the other hand, the $H_{\rm c}$ trend is not regular, but it clearly tends to an increase for the largest values of $t_{\rm w}$ (figure 12(c)).

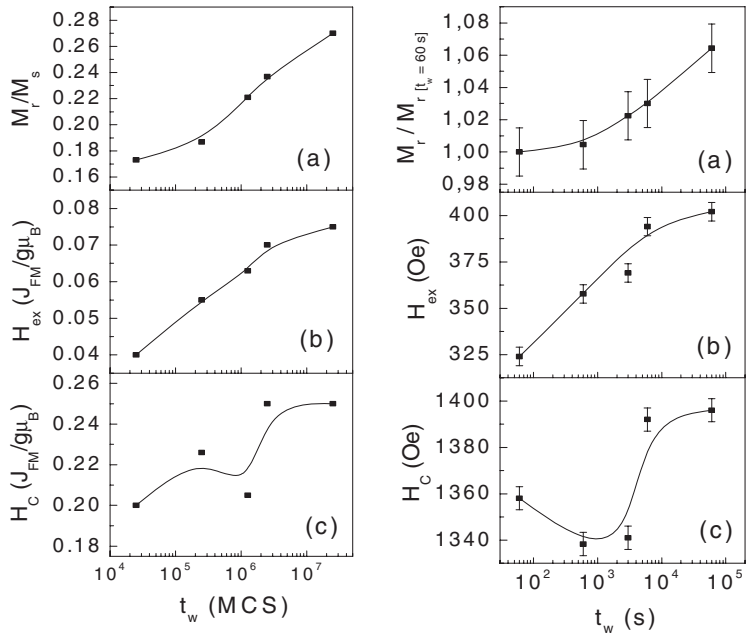

Figure 12. Remanent magnetization M_r (a), exchange field H_{ex} (b) and coercivity H_c (c), as a function of the waiting time t_w. Left panel: the MC simulations; right panel: experimental at $T_f = 5$ K. M_r is normalized to its value at $t_w = 60$ s. The solid line is a guide to the eye.

Then, we studied the effect of the field-cooling rate. The sample was cooled down (cooling rate = 5 K min^{-1}) in zero field from 250 K to $T_i = 50$ K, where $H_{cool} = 4$ kOe was applied; soon after that, the sample was field cooled at a selected rate v_c (between 5 and 0.2 K min^{-1}), down to $T_f = 5$ K and the loop was measured. H_{ex} (figure 13(b)) and M_r (figure 13(a)) increase with decreasing v_c (the change in H_{ex} is ∼18%), whereas H_c does not change significantly (figure 13(c)). The ageing of the system—namely, the increase in the time spent at a temperature at which most of the oxide moments are frozen, either through an increase of t_w at T_i or through a decrease of v_c from T_i to T_f—enhances the EB effect at $T_f = 5$ K. In the first experiment, as t_w elapses at $T_i = 50$ K, the oxide matrix moments relax towards a more stable energy state, in which the interface exchange interaction energy with the moments of the FM component is minimized. Then, with reducing the temperature from T_i to T_f, the system remains trapped in this energy minimum, as it is more difficult to overcome the energy barriers separating different states. It can be easily realized that a similar picture can be drawn for the experiment as a function of v_c.

The above description was confirmed by studying the TRM decay. The sample was cooled down in zero field from $T = 250$ K to $T_i = 50$ K. At T_i, $H_{cool} = 4$ kOe was applied for t_w, before starting the field cooling down to $T_f = 25$ K. At T_f, the field was removed and TRM versus time was measured. Both the curves, measured for $t_w = 0$ s and $t_w = 6000$ s, follow a stretched-exponential decay law, as expected for correlated spin dynamics in disordered systems [26], but the relaxation rate is lower for $t_w = 6000$ s (figure 14(a)).

This confirms the slowing down of the dynamics with increasing t_w and hence the t_w-dependence of the spin configuration of the relaxing disordered phase.

No clear t_w-dependence of TRM was observed at $T_f = 5$ K. The reason is that, at such a low temperature, the relaxation times are too long for an appreciable relaxation to be observed, at

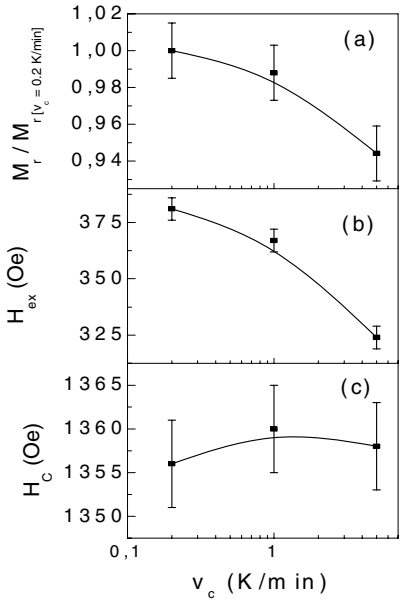

Figure 13. M_r (a), H_{ex} (b) and H_c (c), measured at $T_f = 5$ K, as a function of the cooling rate v_c. M_r is normalized to its value at $v_c = 0.2$ K min^{-1}.

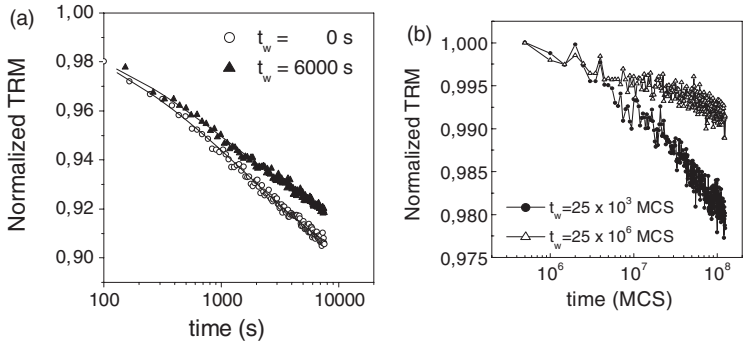

Figure 14. (a) Thermoremanent magnetization (TRM) versus time, at $T_f = 25$ K, for two different t_w values. The TRM is normalized to the value at the beginning of the measurement. The points are fitted to a stretched-exponential decay law (solid line). (b) TRM versus time at $T_f = 0.15$ for two different t_w values, as obtained by the MC simulations. The TRM is normalized to the value at the beginning of the simulation.

least on the investigated timescale. This was in agreement with M_{zfc} versus time measurements, showing no relaxation for $T \leqslant 20$ K. Similarly, no change in H_{ex} was observed after ageing the sample directly at $T_f = 5$ K, rather than at $T_i = 50$ K: at such a low temperature, no appreciable rearrangement in the particle–matrix interface spin configuration occurs, in the investigated timescale. The relaxation process, taking place during t_w, results in a net increase of the oxide magnetization along the cooling field direction, accounting for the small increase in M_r versus t_w, at $T_f = 5$ K (figure 12(a)) (accordingly, M_r increases with decreasing v_c, figure 13(a)). Therefore, by properly ageing the sample, a final spin configuration at $T_f = 5$ K is selected, corresponding to a stronger exchange coupling at the particle–oxide interface, which is responsible for the increase in H_{ex}. In the EB phenomenon, a change in H_{ex} is often

accompanied by a change in H_c [5, 27]. In our case, an enhanced H_c is found after waiting for a long t_w (figure 12(c)), but fluctuating values are measured at shorter t_w and in the case of the measurement as a function of v_c (figure 13(c)). The MC simulation, shown just below, confirms this tendency. H_c is scarcely affected by the ageing effect, as it also depends on intrinsic sources of anisotropy other than exchange anisotropy.

Monte Carlo (MC) simulations have been performed on isolated, spherical core(FM)/shell(FI) nanoparticles simulating the experimental system and procedure followed to investigate the waiting time effect on the EB. We consider spherical nanoparticles of radii R, expressed in lattice spacings, on a simple cubic (sc) lattice, consisting of an FM core and an FI shell, surrounding the core. The spins in the particles interact with nearest-neighbour Heisenberg exchange interaction, and at each crystal site they experience a uniaxial anisotropy. In the presence of an external magnetic field, the total energy of the system is

$$E = -J_{\mathrm{FM}} \sum_{(i,j\in \mathrm{FM})} \vec{S}_i \cdot \vec{S}_j - J_{\mathrm{SH}} \sum_{(i,j\in \mathrm{SH})} \vec{S}_i \cdot \vec{S}_j - \sum_{i\in \mathrm{FM}} K_{i\mathrm{FM}} (\vec{S}_i \cdot \hat{e}_i)^2 - \sum_{i\in \mathrm{SH}} K_{i\mathrm{SH}} (\vec{S}_i \cdot \hat{e}_i)^2 - J_{\mathrm{IF}} \sum_{(i\in \mathrm{FM}, j\in \mathrm{SH})} \vec{S}_i \cdot \vec{S}_j - \vec{H} \cdot \sum_i \vec{S}_i. \tag{3}$$

Here S_i is the atomic spin at site i and $\hat{e}_i$ is the unit vector in the direction of the easy axis at site i. The subscripts IF and SH stand for interface and shell, respectively. The first term gives the exchange interaction between the spins in the FM core (exchange coupling constant J_{FM}, which is taken equal to one). The second term gives the exchange interaction in the FI shell. We set the exchange coupling constant $J_{\mathrm{SH}} = -J_{\mathrm{FM}}/2$ [28]. The third term gives the anisotropy energy of the FM core. If the site i lies in the outer layer of the FM core $K_{i\mathrm{FM}} = K_{\mathrm{IF}}$ and $K_{i\mathrm{FM}} = K_{\mathrm{C}}$ elsewhere. The anisotropy is assumed uniaxial and directed along the z-axis in the whole FM core, including the outer layer facing the FI shell. We take $K_{\mathrm{C}} = 0.05$ and $K_{\mathrm{IF}} = 0.5$, one order of magnitude larger than K_{C}. The fourth term gives the anisotropy energy of the FI shell ($K_{\mathrm{SH}} = 1.5$). If i lies in the outer layer of the shell then $K_{i\mathrm{SH}} = K_{\mathrm{S}} = 1.0$. We consider strong random anisotropy at the interface with the FM core, inside the shell, and at the external surface to model the disordered state of the shell. The fifth term gives the exchange interaction at the interface between the core and the shell. The exchange coupling constant J_{IF} is equal to J_{SH} in size and the interaction is considered ferromagnetic. The last term is the Zeeman energy.

H, H_c and H_{ex} are given in units of $J_{\mathrm{FM}}/g\mu_{\mathrm{B}}$, T in units J_{FM}/k and the anisotropy coupling constants K in units of J_{FM}. M_r is normalized to the magnetization at saturation M_s. The cooling field is $h_L = 0.4$, in our units.

We simulate the field-cooling procedure starting with the nanoparticle at temperature $T = 3.0$ (for the sc lattice the Curie temperature $T_C = 2.9$). The nanoparticle is cooled down to the temperature of 0.75 in zero field. At $T_i = 0.75$, we apply h_L along the z-axis for different waiting times t_w (1, 10, 50, 100, 1000), expressed in Monte Carlo steps per spin (MCSS). Then, we continue the field cooling at a constant rate, down to $T_f = 0.01$, where the loop is measured.

The MC simulations have been performed using the Metropolis algorithm. It should be noted that the time evolution of the system does not come from any deterministic equation for the magnetization. The obtained dynamics is intrinsic to the MC method [29]. This means that our time unit is not related to a real time interval. The results were averaged over 100 different *samples* cooled down under the same conditions (t_w and T_i). M_r, H_{ex} and H_c versus t_w for a particle of radius $R = 9$ and shell thickness three lattice spacings are shown in figure 12 (left panel). The three parameters increase with increasing t_w, satisfactorily reproducing the qualitative features of the experimental results (figure 12, right panel).

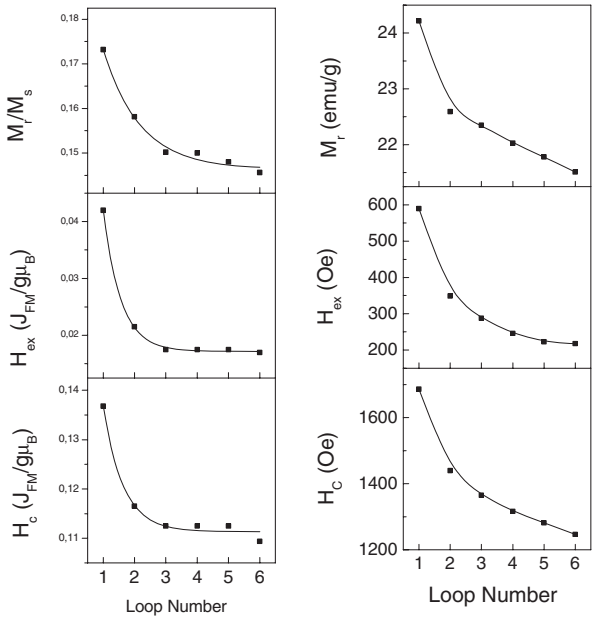

Figure 15. Remanent magnetization M_r (a), exchange field H_{ex} (b) and coercivity H_c (c), as a function of the loop number. Left panel: MC simulations, right panel: experimental values at $T_f = 5$ K. Solid line is only a guide to the eye.

It is worth noticing that the MC simulations also reproduce the experimental TRM decay (figure 14(a)). In figure 14(b), TMR versus time (in MCS) is plotted for two different t_w values, at the temperature $T_f = 0.15$. The decay is slower at higher t_w. Almost no t_w-dependence was observed at lower temperature ($T_f = 0.01$).

The relaxation process, taking place during t_w, results in a net increase of the shell magnetization along the cooling field direction, accounting for the small increase in M_r versus t_w, at $T_f = 5$ K (figure 12). The MC simulations give fluctuating values of H_c at short t_w, as experimentally observed (figure 12(c), left panel).

Simulations were performed considering a shell of four and three lattice spacing thicknesses, maintaining the same core radius. Our results show that there is no effect of shell thickness on the waiting time phenomenon. This is in agreement with MC simulations [28] on F/AF core–shell nanoparticles where it has been demonstrated that at low temperatures, as is the case here, only the first two layers contribute to the exchange bias effect.

Finally, we have repeated the calculations considering for the shell a uniaxial anisotropy directed along the z-axis (except for the external surface, where the anisotropy was assumed to be random). No variation of M_r, H_{ex} and H_c with t_w was observed, revealing that random anisotropy in the shell and at the interface with the FM core is a fundamental ingredient for the appearance of the ageing effect.

2.3.4. The training effect. The training effect [2], i.e. the effect of subsequent hysteresis cycles after field cooling, on EB was investigated. In the literature, the effect (the decrease of H_{ex} with the number of cycles) has been qualitatively attributed to the rearrangement of the interface spin configuration after each hysteresis cycle. However, the detailed microscopic mechanism of such variations is still unclear. The results of experiments at 5 K, after cooling in a field of 4 kOe, are reported in figure 15 (right panel). MC simulations were performed for a

nanoparticle consisting of an FM core and an FI disordered shell. In the simulation, the particle was cooled down to $T = 0.75\ J_{FM}/k$ in zero field and then a field $h_L = 0.4\ J_{FM}/g\mu_B$ was applied down to the temperature $T = 0.01\ J_{FM}/k$. After the removal of this field the hysteresis loop was calculated six times. The procedure is the same as in the experimental situation. The numerical results are reported in figure 15 (left panel). It can be seen that they exhibit the same behaviour. We have also calculated the training effect for a nanoparticle consisting of an FM core and an AFM shell with uniaxial anisotropy directed along the z-axis. In this case the reduction of H_{ex} and H_c is more abrupt than in the previous case as in the F/AF bilayer systems. Our simulations show that in this case only the interface layer contributes to the rearrangement of the spin configuration after the first loop. In the FM/FI nanoparticle case the core spins contribute also in the training effect and this produces the different behaviour.

3. Conclusions

In conclusion, our results show that magneto-thermal history and dynamical effects have a sizeable influence on the EB properties of the nanogranular disordered Fe/FeO_x material, an example of FM/'SG-like' system. It was found that H_{ex}, H_c and M_r are strongly affected by the cooling field value, H_{cool}, and that they can also be controlled by varying the waiting time, t_w, at the initial cooling temperature and the cooling rate, v_c. This is related to the inherent magnetic disorder of the oxide phase, implying many equivalent spin configurations. Through the variation of H_{cool}, t_w and v_c, one can select the final frozen spin configuration of the disordered oxide phase at the interface with the ordered Fe component. The waiting time dependence of H_{ex}, H_c and M_r is confirmed by MC simulations on core(FM)/shell(FI) nanoparticles showing the presence of a spin-glass-like dynamics for the EB properties, provided that a shell random anisotropy is assumed. The possibility of a fine control of $H_{ex}(H_c, M_r)$ in this kind of system opens perspectives for technological applications in tuning the performance of EB-based magnetic devices.

Acknowledgments

The research was sponsored by the Italian Ministry of Education, University and Research (MIUR) under project FIRB 'Microsystems based on novel magnetic materials structured on a nanoscopic scale'. The support of the EU under NANOSPIN Contract No. NMP4-CT-2004-013545 is also acknowledged.

References

[1] Meiklejohn W H and Bean C P 1957 *Phys. Rev.* **102** 1413
[2] Nogues J and Schuller I K 1999 *J. Magn. Magn. Mater.* **192** 203
[3] Kodama R H, Berkowitz A E, McNiff E J and Foner S 1996 *Phys. Rev. Lett.* **77** 394
[4] Kodama R H, Makhlouf SA and Berkowitz A E 1997 *Phys. Rev. Lett.* **79** 1393
[5] Binder K and Young A P 1986 *Rev. Mod. Phys.* **58** 801
[6] Del Bianco L, Fiorani D, Testa A M, Bonetti E and Signorini L 2004 *Phys. Rev.* B **70** 052401
[7] Refregier Ph, Vincent E, Hammann J and Ocio M 1987 *J. Physique* **48** 1533
[8] Jonsson T, Mattsson J, Djurberg C, Khan F A, Nordblad P and Svedlindh P 1995 *Phys. Rev. Lett.* **75** 4138
[9] Birringer R, Gleiter H, Klein H P and Marquardt P 1984 *Phys. Lett.* A **102** 365
[10] Del Bianco L, Fiorani D, Testa A M, Bonetti E, Savini L and Signoretti S 2002 *Phys. Rev.* B **66** 174418
[11] Rietveld H M 1966 *Acta Crystallogr.* **20** 508
[12] Haneda K and Morrish A H 1979 *Nature* **282** 186

[13] Gangopadhyay S, Hadjipanayis G C, Dale B, Sorensen C M, Klabunde K J, Papaefthymiou V and Kostikas A 1992 *Phys. Rev.* B **45** 9778
[14] Coey J M 1971 *Phys. Rev. Lett.* **27** 1140
[15] Tronc E, Ezzir A, Cherkaoui R, Chanéac C, Noguès M, Kachkachi H, Fiorani D, Testa A M, Grenèche J M and Jolivet J P 2000 *J. Magn. Magn. Mater.* **221** 63
[16] O'Grady K and Chantrell R W 1992 *Magnetic Properties of Fine Particles* ed J L Dormann and D Fiorani (Amsterdam: North-Holland) p 93
[17] Zhang P, Zuo F, Urban F K III, Khabari A, Griffiths P and Hosseini-Tehrani A 2001 *J. Magn. Magn. Mater.* **225** 337
[18] Stoner E C and Wohlfarth E P 1948 *Proc. Phys. Soc.* A **240** 599
[19] Loffler J F, Meier J P, Doudin B, Ansermet J P and Wagner W 1998 *Phys. Rev.* B **57** 2915
[20] Meiklejohn W H 1962 *J. Appl. Phys.* **33** 1328
[21] Martinez B, Roig A, Obradors X, Molins E, Rouanet A and Monty C 1996 *J. Appl. Phys.* **79** 2580
[22] Martinez B, Obradors X, Balcells Ll, Rouanet A and Monty C 1998 *Phys. Rev. Lett.* **80** 181
[23] Nogues J, Lederman D, Moran T J and Schuller I K 1996 *Phys. Rev. Lett.* **76** 4624
[24] Lyberatos A, Earl J and Chantrell R W 1996 *Phys. Rev.* E **53** 5493
[25] Toloza J H, Tamarit F A and Cannas S A 1998 *Phys. Rev.* B **58** R8885
[26] Chamberlin R V, Mozurkewich G and Orbach R 1984 *Phys. Rev. Lett.* **52** 867
[27] Dimitrov D V, Zhang S, Xiao J Q, Hadjipanayis G C and Prados C 1998 *Phys. Rev.* B **58** 12090
[28] Eftaxias E and Trohidou K N 2005 *Phys. Rev.* B **71** 134406
[29] Gonzalez J M, Chubykalo O A and Smirnov-Rueda R 1999 *J. Magn. Magn. Mater.* **203** 18